Synthesis, Structure, and Thermotropic Mesomorphism of Layered *N*-Alkylpyridinium Tetrahalopalladate(II) Salts

Francesco Neve,* Alessandra Crispini, and Salvatore Armentano

Dipartimento di Chimica, Università della Calabria, I-87030 Arcavacata di Rende (CS), Italy

Oriano Francescangeli

Dipartimento di Scienze dei Materiali e della Terra, Sezione Fisica, Università di Ancona, Via Brecce Bianche, I-60131 Ancona, Italy

Received February 5, 1998. Revised Manuscript Received April 23, 1998

Two homologous series of *N*-alkylpyridinium salts, $[Cn\text{-}Py]_2[PdX_4]$ (n = 12, 14, 16, 18; X = Cl, Br), have been synthesized, and their thermal behavior has been studied by differential scanning calorimetry and hot-stage polarizing optical microscopy. Except for the substances with n = 12, all the materials show thermotropic polymorphism. The crystal structures of $[C12\text{-}Py]_2[PdCl_4]$, $[C16\text{-}Py]_2[PdCl_4]$, and $[C16\text{-}Py]_2[PdBr_4]$ have been solved. All three complex salts crystallize in the triclinic space group $P\bar{1}$. Crystal packing reveals layered structures with alternating polar and apolar sublayers, where each $[PdX_4]^{2-}$ anion is sandwiched between two antiparallel pyridinium cations. Alkyl chains are highly interdigitated and tilted with respect to the layer normal. The structural characterization of the $[Cn\text{-}Py]_2[PdX_4]$ (n = 16, 18; X = Cl, Br) salts has been achieved also through variable-temperature powder X-ray diffraction. The $[PdCl_4]^{2-}$ salts undergo transitions to a second crystalline phase and then to an ordered and a disordered smectic phase. The latter are assigned to single-layered smectic-E and partially bilayered smectic-A_d phases, respectively. On warming, the $[PdBr_4]^{2-}$ analogues only show the smectic-A_d phase, preceded by a crystalline phase very similar to the room-temperature solid phase. The relative importance of hydrogen bonding throughout the sequence of structural changes is briefly addressed.

Introduction

Organic cations bearing long hydrocarbon chains attract steady interest, mainly due to the low-dimensional solid-state features of their salts. Currently, they are studied for uses as diverse as structure-directing agents for mesoporous materials,[1,2] reagents for vapor deposition of quantum-well structures,[3] models for lipid bilayer systems,[4] or promesogenic building blocks for thermotropic liquid crystalline materials.[5,6]

Because of their amphiphilic character, the salts of long-chain organic cations usually have a room-temperature, lipid-like bilayer structure (consisting of alternating ionic and paraffinic, nonpolar sublayers) which on heating undergoes structural phase transitions, some of which may lead to mesophase formation. A classical example of such thermotropic behavior is seen in simple alkylammonium salts.[7] Among them, an interesting subclass is represented by $[RNH_3]_2[MX_4]$ species (M = divalent metal, X = halide) which display two different structural motifs in the ionic sublayer dependent on the metal.[8−10] Whereas metal cations with a strong preference for octahedral coordination (Mn, Fe, Cu, Hg, Cd) will form corner-sharing MX_6 octahedra arranged in a perovskite-type infinite sheet, other metals (e.g., Co, Pd, Zn) will contribute to the crystal packing with isolated $[MX_4]^{2-}$ ions. Short- and long-range Coulomb forces

* Please address correspondence to this author. E-mail: f.neve@unical.it.

(1) (a) Kresge, C. T.; Leonowicz, M. E.; Roth, W. J.; Vartuli, J. C.; Beck, J. S. *Nature* **1991**, *359*, 710. (b) Beck, J. S.; Vartuli, J. C.; Roth, W. J.; Leonowicz, M. E.; Kresge, C. T.; Schmitt, K. T.; Chu, C. T.-W.; Olson, D. H.; Sheppard, E. W.; McCullen, S. B.; Higgins, J. B.; Schlenker, J. L. *J. Am. Chem. Soc.* **1992**, *114*, 10834.

(2) For a recent example, see Huo, Q.; Feng, J.; Schuth, F.; Stucky, G. D. *Chem. Mater.* **1997**, *9*, 14.

(3) Era, M.; Hattori, T.; Taira, T.; Tsutsui, T. *Chem. Mater.* **1997**, *9*, 8 and references therein.

(4) Kanazawa, A.; Tsutsumi, O.; Ikeda, T.; Nagase, Y. *J. Am. Chem. Soc.* **1997**, *119*, 7670.

(5) (a) Bowlas, C. J.; Bruce, D. W.; Seddon, K. R. *Chem. Commun.* **1996**, 1625.

(6) Lee, K. M.; Lee, C. K.; Lin, I. J. B. *Chem. Commun.* **1997**, 899.

(7) (a) Malliaris, A.; Christias, C.; Margomenou-Leonidopoulou, G.; Paleos, C. M. *Mol. Cryst. Liq. Cryst.* **1982**, *82*, 161. (b) Busico, V.; Corradini, P.; Vacatello, M. *J. Phys. Chem.* **1982**, *86*, 1033. (c) Busico, V.; Cernicchiaro, P.; Corradini, P.; Vacatello, M. *J. Phys. Chem.* **1983**, *87*, 1631. (d) Margomenou-Leonidopoulou, G.; Malliaris, A.; Paleos, C. M. *Termochim. Acta* **1985**, *85*, 147. (e) Gault, J. D.; Gallardo, H. A.; Muller, H. J. *Mol. Cryst. Liq. Cryst.* **1985**, *130*, 163. (f) Margomenou-Leonidopoulou, G. *Termochim. Acta* **1988**, *134*, 49.

(8) (a) Vacatello, M.; Corradini, P. *Gazz. Chim. Ital.* **1973**, *103*, 1027. (b) Vacatello, M.; Corradini, P. *Gazz. Chim. Ital.* **1974**, *104*, 773. (c) Landi, E.; Vacatello, M. *Termochim. Acta* **1975**, *12*, 141. (d) Landi, E.; Vacatello, M. *Termochim. Acta* **1975**, *13*, 441. (e) Salerno, V.; Grieco, A.; Vacatello, M. *J. Phys. Chem.* **1976**, *80*, 2444. (f) Landi, E.; Salerno, V.; Vacatello, M. *Gazz. Chim. Ital.* **1977**, *107*, 27. (g) Busico, V.; Castaldo, D.; Vacatello, M. *Mol. Cryst. Liq. Cryst.* **1981**, *78*, 221.

(9) Bocanegra, E. H.; Tello, M. J.; Arriandaga, M. A.; Arend, H. *Solid State Commun.* **1975**, *17*, 1221.

(10) Needham, G. F.; Willett, R. D.; Franzen, H. F. *J. Phys. Chem.* **1984**, *88*, 674.

S0897-4756(98)00071-4 CCC: $15.00
Published on Web 06/20/1998

coupled with weak hydrogen bonding keep cations and anions in place, while dispersive forces guide the buildup of the apolar regions. Definitive structural proofs have been obtained for M = Mn,[11] Zn,[12] and Cd.[13]

Other quaternary ammonium salts containing an aromatic core such as pyridinium,[5,14−19] imidazolium,[5,6] and benzimidazolium[6] salts give rise to bilayered structures with various degrees of interdigitation of the alkyl chains. But, while most salts of cationic amphiphiles possessing a rigid core contain simple halides as counterions, a recent report addressed the thermotropic liquid crystalline properties of *N*-alkylpyridinium [C*n*-Py]$^+$ (n = 12, 14, 16, 18) cations where the counterion was a tetrahedral tetrachlorometalate $[MCl_4]^{2-}$ ion (M = Co, Ni).[5] Since some of the lower homologues of the above ammonium cations are essential for the important class of organochloroaluminate ionic liquids,[20,21] the authors envisaged a possible use as solvents for the low-melting liquid crystalline higher homologues.[5]

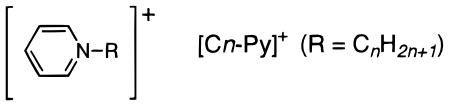

As part of our ongoing work on thermotropic ionic metal complexes,[22] we thought it would be of interest to extend the range of complex metal anions, while maintaining the same type of cation (namely, pyridinium). This approach should enable us to study the influence of varying the size, type, and geometry of the $[MX_4]^{2-}$ anion on the liquid crystalline properties of species of the type [C*n*-Py]$_2$[MX_4]. We therefore undertook the synthesis of two homologous series of long-chain *N*-alkylpyridinium tetrahalopalladate salts. Here we present the results of the thermal, optical, and structural characterization of this new class of thermotropic ionic liquid crystals.

Experimental Section

General Methods. The pyridinium halides [C12-Py][Cl], [C16-Py][Cl], and [C16-Py][Br] are commercially available (Aldrich) as monohydrate salts. $PdCl_2$ was supplied by Fluka. ^{1}H NMR spectra in $CDCl_3$ solution with tetramethylsilane as the internal standard were obtained on a Bruker WH300 spectrometer operating at 300 MHz. Elemental analyses were performed at the Microanalytical Laboratory of the Università della Calabria.

Optical observations were carried out with a Zeiss Axioskop polarizing microscope equipped with a Linkam CO 600 heating stage and a temperature control unit. Phase transition temperatures were measured by differential scanning calorimetry (DSC) with a Perkin-Elmer DSC-7 instrument operating at a scanning rate of 10 °C/min unless otherwise stated. Transition temperatures were taken as a peak top.

Variable-temperature X-ray diffraction (VT-XRD) measurements on powdered samples were performed with an INEL CPS 120 powder diffractometer equipped with a position-sensitive detector covering 120° in the scattering angle 2θ, with an angular resolution of 0.018°. Monochromatized Cu Kα (λ = 1.54 Å) radiation was used. The samples, ~1 mm thick, were placed between two thin Al sheets, fixed to a circular hole (1 cm diameter) in an Al sample holder. Heating was achieved by use of a hot stage with stability control ± 0.1 °C.

X-ray diffraction data on single crystals were collected on a Siemens R3m/V four-circle diffractometer with graphite monochromated Mo Kα radiation (λ = 0.71073 Å).

Synthesis of the Pyridinium Salts. (A) Pyridinium Halides, [C*n*-Py][X]. The salts that were not commercially available were prepared as monohydrate species following a procedure reported by Skoulios et al. for related *N*-alkylpyridinium salts[15c] with slight modifications. The bromides were prepared in dry pyridine under reflux conditions to obtain shorter reaction times (4 h), and pure compounds were available in very good yield (>90%) after a single recrystallization from pyridine−diethyl ether. Chloride salts were available from the bromide analogues by reaction with silver chloride[15c] and subsequent recrystallization from pyridine−diethyl ether (quantitative yield). Typical ^{1}H NMR spectral data are given for [C14-Py][Cl]: δ 9.53 (d, 2H, J = 5.8 Hz), 8.47 (t, 1H, J = 7.8 Hz), 8.12 (br t, 2 H), 5.01 (t, 2 H, J = 7.4 Hz), 2.11 (s, 2 H, H_2O), 2.02 (m, 2 H), 1.31−1.21 (m, 22 H), 0.86 (t, 3H).

(B) Tetrahalopalladate Pyridinium Salts, [C*n*-Py]$_4$[PdX$_4$] (n = 12, 14, 16, 18; X = Cl, Br). The series of [C*n*-Py]$_2$[$PdCl_4$] salts was synthesized by reaction of 2 equiv of the appropriate pyridinium chloride [C*n*-Py][Cl] with $PdCl_2$ (0.05 g, 0.28 mmol) in refluxing acetonitrile (15 mL) for 30 min. A microcrystalline pinkish-brown product was always obtained upon cooling of the reaction mixture. Yields were in the range 70−90%.

The bromide analogues [C*n*-Py]$_2$[$PdBr_4$] were prepared in a similar manner following a preliminary metathetical exchange. A warm solution of $PdCl_2$ (0.05 g, 0.28 mmol) in acetonitrile (15 mL) was treated with a saturated aqueous solution of a 10-fold molar excess of KBr. After 10 min of stirring, 2 equiv of the appropriate pyridinium bromide [C*n*-Py][Br] was added to the red solution, and the reaction mixture was heated to reflux for another 30 min. Cooling of the resulting solution afforded the expected product as a red-brown

(11) Ciajolo, M. R.; Corradini, P.; Pavone, V. *Gazz. Chim. Ital.* **1976**, *106*, 807.
(12) Ciajolo, M. R.; Corradini, P.; Pavone, V. *Acta Crystallogr.* **1977**, *B33*, 553.
(13) Kind, R.; Plesko, S.; Arend, H.; Blinc, R.; Zeks, B.; Seliger, J.; Lozar, B.; Slak, J.; Levstik, A.; Filipic, C.; Zagar, V.; Lahajnar, G.; Milia, F.; Chapuis, G. *J. Phys. Chem.* **1979**, *71*, 2118.
(14) Knight, G. A.; Show, B. D. *J. Chem. Soc.* **1936**, 682.
(15) (a) Bazuin, C. G.; Guillon, D.; Skoulios, A.; Nicoud, J. F. *Liq. Cryst.* **1986**, *1*, 181. (b) Bazuin, C. G.; Guillon, D.; Skoulios, A.; Zana, R. *J. Phys. (France)* **1986**, *47*, 927. (c) Navarro-Rodriguez, D.; Frere, Y.; Gramain, P.; Guillon, D.; Skoulios, A.; Nicoud, J. F. *Liq. Cryst.* **1991**, *9*, 321. (d) Bruce, D. W.; Estdale, S.; Guillon, D.; Heinrich, B. *Liq. Cryst.* **1995**, *19*, 301.
(16) (a) Sudholter, E. J. R.; Engherts, J. B. F. N.; de Jeu, W. H. *J. Phys. Chem.* **1982**, *86*, 1908. (b) Nusselder, J. J. H.; Engherts, J. B. F. N.; Van Doren, H. A. *Liq. Cryst.* **1993**, *13*, 213.
(17) Somashekar, R. *Mol. Cryst. Liq. Cryst.* **1987**, *146*, 225.
(18) Kosaka, Y.; Kato, T.; Uryu, T. *Liq. Cryst.* **1995**, *18*, 693.
(19) (a) Haramoto, Y.; Ujiie, S.; Nanasawa, M. *Liq. Cryst.* **1996**, *21*, 923. (b) Haramoto, Y.; Akiyama, Y.; Segawa, R.; Ujiie, S.; Nanasawa, M. *J. Mater. Chem.* **1998**, *8*, 275.
(20) Hussey, C. L. *Pure Appl. Chem.* **1988**, *60*, 1763.
(21) Chauvin, Y.; Olivier-Bourbigou, H. *CHEMTECH* **1995**, *25* (9), 26.
(22) (a) Neve, F.; Ghedini, M.; Levelut, A.-M.; Francescangeli, O. *Chem. Mater.* **1994**, *6*, 70. (b) Neve, F.; Ghedini, M.; De Munno, G.; Levelut, A.-M. *Chem. Mater.* **1995**, *7*, 688. (c) Neve, F. *Adv. Mater.* **1996**, *8*, 277.

Table 1. Microanalytical Data for the Halide and Tetrahalopalladate Pyridinium Salts

compd	calcd (found) (%) C	H	N
[C14-Py][Cl]·H_2O	69.67 (69.17)	11.31 (11.00)	4.40 (4.24)
[C18-Py][Cl]·H_2O	71.56 (72.29)	11.49 (11.82)	3.63 (4.00)
[C12-Py][Br]·H_2O	58.95 (58.71)	9.31 (9.25)	4.04 (4.24)
[C14-Py][Br]·H_2O	60.95 (60.65)	9.69 (9.64)	3.74 (3.92)
[C18-Py][Br]·H_2O	64.17 (63.51)	10.30 (10.21)	3.25 (2.95)
[C12-Py]$_2$[$PdCl_4$]	54.81 (54.38)	8.10 (8.10)	3.76 (3.96)
[C14-Py]$_2$[$PdCl_4$]	56.97 (57.18)	8.55 (8.73)	3.49 (3.80)
[C16-Py]$_2$[$PdCl_4$]	58.71 (58.50)	9.15 (8.85)	3.26 (3.56)
[C18-Py]$_2$[$PdCl_4$]	60.48 (59.94)	9.27 (9.30)	3.07 (3.10)
[C12-Py]$_2$[$PdBr_4$]	44.25 (44.51)	6.55 (6.67)	3.03 (3.18)
[C14-Py]$_2$[$PdBr_4$]	46.62 (47.15)	7.00 (7.21)	2.86 (2.80)
[C16-Py]$_2$[$PdBr_4$]	48.73 (48.35)	7.40 (7.46)	2.70 (2.70)
[C18-Py]$_2$[$PdBr_4$]	50.63 (50.27)	7.75 (7.77)	2.56 (2.61)

Table 2. Crystallographic Data for Complexes [C12-Py]$_2$[$PdCl_4$], [C16-Py]$_2$[$PdCl_4$], and [C16-Py]$_2$[$PdBr_4$]

	[C12-Py]$_2$[$PdCl_4$]	[C16-Py]$_2$[$PdCl_4$]	[C16-Py]$_2$[$PdBr_4$]
chemical formula	$C_{34}H_{60}N_2Cl_4Pd$	$C_{42}H_{76}N_2Cl_4Pd$	$C_{42}H_{76}N_2Br_4Pd$
formula weight	745.0	857.2	1035.1
space group	$P\bar{1}$	$P\bar{1}$	$P\bar{1}$
a, Å	7.416(2)	7.846(4)	7.965(3)
b, Å	8.082(2)	8.068(4)	8.207(2)
c, Å	17.222(7)	19.088(8)	19.046(5)
α, deg	88.22(3)	96.07(4)	96.11(2)
β, deg	79.08(2)	93.05(4)	93.65(3)
γ, deg	76.47(2)	103.99(4)	105.04(3)
V, Å^3	985.3(5)	1162.0(10)	1190.1(6)
Z	1	1	1
T, °C	25	25	25
λ, Å	0.71073	0.71073	0.71073
D_{calcd}, g cm^{-3}	1.256	1.225	1.444
μ, mm^{-1}	0.765	6.580	3.775
R^a	0.0527	0.0683	0.0542
$R_w{}^b$	0.0642	0.0646	0.0570

[a] $R = \sum||F_o| - |F_c||/\sum|F_o|$. [b] $R_w = [\sum w(|F_o| - |F_c|)^2/\sum w|F_o|^2]^{1/2}$.

microcrystalline solid. Yields were in the range 68−85%.

Except for the absent water signal, ^{1}H NMR spectra of the [C*n*-Py]$_2$[PdX_4] species are similar to those observed for the parent halide salts, and they are not reported here. The purity of the two series of [C*n*-Py]$_2$[PdX_4] species was also checked by elemental analysis. The microanalytical data for the synthesized halide and tetrahalopalladate pyridinium salts are gathered in Table 1.

X-ray Crystal Structure Determination. Crystal data for [C12-Py]$_2$[$PdCl_4$], [C16-Py]$_2$[$PdCl_4$], and [C16-Py]$_2$[$PdBr_4$] with details of the structure solution and refinement are summarized in Table 2. The data were corrected for Lorentz, polarization, and X-ray absorption effects, and an empirical absorption correction was applied using a method based upon azimuthal (Ψ) scan data.[23] The structures were solved by Patterson and Fourier methods and refined by full-matrix least-squares refinement. All the non-hydrogen atoms were refined anisotropically, and the hydrogen atoms were included as idealized atoms riding on the respective carbon atoms with C−H bond lengths appropriate to the carbon atom hybridization. The isotropic displacement parameter of each hydrogen atom was fixed at $U = 0.08$ Å^2. The weighting scheme used in the last refinement cycle was $w^{-1} = \sigma^2|F_o| + q|F_c|^2$, with $q = 0.0025$ for [C12-Py]$_2$[$PdCl_4$] and $q = 0.0010$ for [C16-Py]$_2$[$PdCl_4$] and [C16-Py]$_2$[$PdBr_4$]. All calculations were performed with the programs SHELXTL PLUS[24] and PARST.[25] Atomic scattering factors were as implemented in SHELXTL PLUS. Atomic positional parameters are shown in Table 3.

Results

Synthesis and X-ray Crystal Structures. The chemical synthesis of the [C*n*-Py]$_2$[$PdCl_4$] complex salts is straightforward and consists of a single reaction between $PdCl_2$ and the appropriate *N*-alkylpyridinium chloride (molar ratio 1:2) in refluxing acetonitrile. Cooling of the reaction mixture invariably gives a microcrystalline product. Yields increase with *n*, matching the corresponding decrease of solubility in the polar solvent. The homologous series [C*n*-Py]$_2$[$PdBr_4$] is obtained in a similar manner provided $PdBr_2$ is prepared in situ from $PdCl_2$. [C*n*-Py]$_2$[PdX_4] (X = Cl, Br) salts are obtained as anhydrous solids (although no special care was used to exclude water) that can be stored indefinitely in air.

Single crystals of [C12-Py]$_2$[$PdCl_4$], [C16-Py]$_2$[$PdCl_4$], and [C16-Py]$_2$[$PdBr_4$] were obtained from acetonitrile, and their molecular structures were determined by X-ray diffraction. The molecular structure of [C12-Py]$_2$[$PdCl_4$] is shown in Figure 1. The three complex salts crystallize in the triclinic space group $P\bar{1}$ but while complexes [C16-Py]$_2$[$PdCl_4$] and [C16-Py]$_2$[$PdBr_4$] are practically isomorphous, the presence of a shorter aliphatic chain in complex [C12-Py]$_2$[$PdCl_4$] causes a shortening of the *c*-axis. In all cases, the organic cations in the unit cell are centrosymmetrically arranged around the $[PdX_4]^{2-}$ anion, with the Pd atom lying on the inversion center.

The molecular structures exhibit normal geometry. The bond lengths and bond angles of the organic cation are found to be in good agreement with those found in other pyridinium salts.[26] Table 4 reports selected bonding parameters. The conformation of the hydrocarbon chain is almost completely *trans*-planar (average torsion angles of 178.1(9)° for [C12-Py]$_2$[$PdCl_4$], 177.4(8)° for [C16-Py]$_2$[$PdCl_4$], and 177.8(6)° for [C16-Py]$_2$[$PdBr_4$]). The $[PdX_4]^{2-}$ anions are in a regular square-planar geometry, the average X-Pd-X angle being 90.0(1)° in all complexes. The coordination plane of the $[PdX_4]^{2-}$ anion is nearly orthogonal to the mean plane of the pyridine ring, with dihedral angles of 98.0(2)° for [C12-Py]$_2$[$PdCl_4$], 92.1(2)° for [C16-Py]$_2$[$PdCl_4$], and 96.6(2)° for [C16-Py]$_2$[$PdBr_4$].

The crystal packing, driven by the Coulombic interactions, in all three complex salts has cation molecules arranged in an antiparallel fashion which give rise to a layered structure with alternating polar and apolar

(23) North, A. C. T.; Phillips, D. C. *Acta Crystallogr. A* **1968**, *24*, 351.

(24) *SHELXTL PLUS*, version 4.21; Siemens Analytical X-ray Instruments, Inc.: Madison, WI, 1990.

(25) Nardelli, M. *Comput. Chem.* **1983**, *7*, 95.

(26) (a) Ward, D. L.; Rhinebarger, R. R.; Popov, A. I. *Acta Crystallogr.* **1986**, *C42*, 1771. (b) Zaworotko, M. J.; Cameron, T. S.; Linden, A.; Sturge, K. C. *Acta Crystallogr.* **1989**, *C45*, 996. (c) Narula, S. P.; Kaur, S.; Sharma, S. K.; Povey, D. C. *J. Crystallogr. Spectrosc. Res.* **1992**, *22*, 139. (d) Paradies, H. H.; Habben, F. *Acta Crystallogr.* **1993**, *C49*, 744. (e) Virovets, A. V.; Vakulenko, N. N.; Volkov, V. V.; Podberezkaya, N. V. *Zh. Strukt. Khim.* **1994**, *35*, 72. (f) Vongbupnimit, K.; Noguchi, K.; Okuyama, K. *Acta Crystallogr.* **1995**, *C51*, 1940.

Table 3. Atomic Positional Parameters ($\times 10^4$) and Equivalent Isotropic Displacement Coefficients ($Å^2 \times 10^3$) for $[C12\text{-}Py]_2[PdCl_4]$, $[C16\text{-}Py]_2[PdCl_4]$, and $[C16\text{-}Py]_2[PdBr_4]$

	x	*y*	*z*	U_{eq}
		$[C12\text{-}Py]_2[PdCl_4]$		
Pd	0	0	0	43(1)
Cl(1)	−947(3)	−2406(3)	−252(1)	78(1)
Cl(2)	−1438(3)	−19(2)	1313(1)	70(1)
N	3673(8)	4391(7)	−1391(3)	52(2)
C(1)	4615(10)	2868(10)	−1169(5)	63(3)
C(2)	6255(12)	2700(13)	−903(6)	85(4)
C(3)	6948(12)	4073(17)	−833(6)	91(5)
C(4)	5954(15)	5638(15)	−1026(6)	87(5)
C(5)	4345(13)	5769(10)	−1310(5)	71(4)
C(6)	1930(9)	4509(10)	−1697(5)	61(3)
C(7)	2334(11)	3890(11)	−2536(5)	72(4)
C(8)	522(12)	3945(13)	−2825(6)	88(4)
C(9)	647(14)	3279(14)	−3621(6)	94(5)
C(10)	−1138(13)	3305(13)	−3889(6)	89(4)
C(11)	−1144(15)	2624(15)	−4672(6)	97(5)
C(12)	−2939(14)	2694(14)	−4917(6)	96(5)
C(13)	−3030(15)	1986(15)	−5681(7)	109(6)
C(14)	−4839(16)	2093(15)	−5912(7)	106(5)
C(15)	−5065(15)	1354(15)	−6620(7)	104(5)
C(16)	−6853(19)	1486(20)	−6836(8)	146(8)
C(17)	−7111(19)	732(17)	−7522(8)	130(7)
		$[C16\text{-}Py]_2[PdCl_4]$		
Pd	0	0	0	39(1)
Cl(1)	−1178(3)	2231(3)	−275(1)	66(1)
Cl(2)	943(4)	−233(3)	−1121(2)	75(1)
N	−3126(9)	4688(9)	1161(4)	54(3)
C(1)	−4031(12)	3063(11)	939(5)	56(4)
C(2)	−5798(13)	2737(13)	707(6)	66(4)
C(3)	−6600(12)	4071(15)	703(6)	71(5)
C(4)	−5640(14)	5701(15)	910(6)	76(5)
C(5)	−3902(13)	6000(12)	1160(6)	65(4)
C(6)	−1256(11)	5004(12)	1437(5)	58(4)
C(7)	−1062(11)	4369(12)	2145(5)	56(4)
C(8)	861(11)	4703(12)	2403(6)	63(4)
C(9)	1217(12)	3783(12)	3026(5)	58(4)
C(10)	3103(12)	4163(12)	3303(6)	63(4)
C(11)	3542(12)	3119(11)	3861(5)	58(4)
C(12)	5491(12)	3521(11)	4114(6)	64(4)
C(13)	5927(11)	2463(11)	4668(6)	63(4)
C(14)	7847(12)	2889(11)	4933(5)	60(4)
C(15)	8327(12)	1795(11)	5488(5)	58(4)
C(16)	10238(12)	2228(12)	5730(6)	59(4)
C(17)	10712(12)	1164(12)	6305(5)	59(4)
C(18)	12654(12)	1606(12)	6533(6)	62(4)
C(19)	13193(12)	549(12)	7074(5)	60(4)
C(20)	15130(13)	1025(13)	7305(5)	63(4)
C(21)	15644(15)	22(14)	7855(7)	91(5)
		$[C16\text{-}Py]_2[PdBr_4]$		
Pd	0	0	0	34(1)
Br(1)	−712(1)	355(1)	1222(1)	64(1)
Br(2)	−1228(1)	2292(1)	−268(1)	66(1)
N	−3080(6)	4749(6)	1221(3)	43(2)
C(1)	−3787(10)	6038(9)	1203(4)	61(3)
C(2)	−5517(11)	5768(11)	958(5)	72(3)
C(3)	−6519(10)	4110(11)	741(4)	69(3)
C(4)	−5741(10)	2808(10)	768(4)	62(3)
C(5)	−4035(9)	3135(8)	990(4)	52(3)
C(6)	−1224(8)	5058(9)	1495(4)	54(3)
C(7)	−1044(8)	4463(9)	2220(3)	49(2)
C(8)	879(9)	4795(9)	2482(4)	59(3)
C(9)	1220(8)	3839(9)	3086(4)	53(3)
C(10)	3139(8)	4202(9)	3334(4)	54(3)
C(11)	3569(9)	3149(9)	3886(4)	55(3)
C(12)	5503(8)	3551(9)	4131(4)	53(3)
C(13)	5944(8)	2470(9)	4688(4)	54(3)
C(14)	7861(8)	2884(9)	4933(4)	52(3)
C(15)	8306(8)	1802(9)	5477(4)	54(3)
C(16)	10255(9)	2234(8)	5720(4)	52(3)
C(17)	10705(8)	1137(9)	6265(4)	52(3)
C(18)	12638(9)	1573(9)	6495(4)	55(3)
C(19)	13144(9)	486(9)	7025(4)	53(3)
C(20)	15086(9)	987(10)	7262(4)	63(3)
C(21)	15589(12)	−70(12)	7812(5)	80(4)

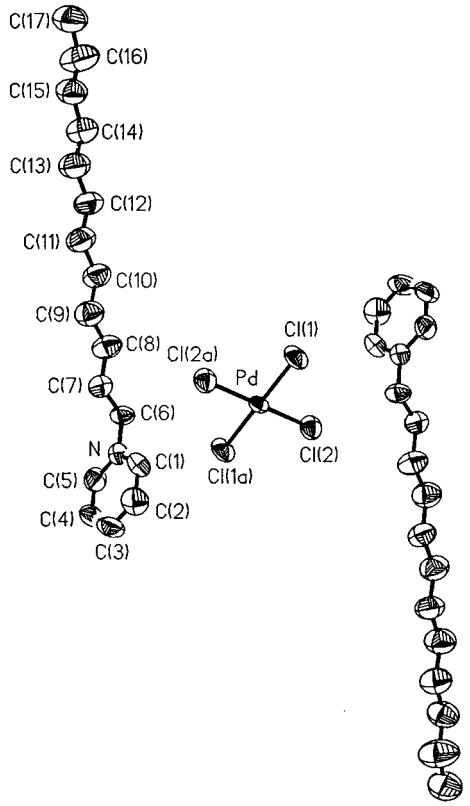

Figure 1. Molecular structure of $[C12\text{-}Py]_2[PdCl_4]$ with the atomic numbering scheme. Thermal ellipsoids are shown at the 50% level. Hydrogens have been omitted for clarity.

Table 4. Selected Bond Lengths (Å) and Angles (deg) for $[C12\text{-}Py]_2[PdCl_4]$, $[C16\text{-}Py]_2[PdCl_4]$, and $[C16\text{-}Py]_2[PdBr_4]$

		$[C12\text{-}Py]_2[PdCl_4]$	
Pd−Cl(1)	2.295 (3)	Cl(1)−Pd-Cl(2)	90.7(1)
Pd−Cl(2)	2.311 (2)	Cl(1)−Pd−Cl(2a)	89.3(1)
N−C(1)	1.349 (9)	C(1)−N−C(5)	118.7(7)
N−C(5)	1.343 (11)	C(1)−N−C(6)	119.5(7)
N−C(6)	1.467 (10)	C(5)−N−C(6)	121.8(6)
C(1)−C(2)	1.356 (13)	N−C(1)−C(2)	121.3(8)
C(2)−C(3)	1.345 (17)	N−C(5)−C(4)	121.0(8)
C(3)−C(4)	1.373 (16)	C(1)−C(2)−C(3)	120.2(9)
C(4)−C(5)	1.354 (16)	C(2)−C(3)−C(4)	118.8(10)
		C(3)−C(4)−C(5)	119.9(11)
		$[C16\text{-}Py]_2[PdCl_4]$	
Pd−Cl(1)	2.307 (3)	Cl(1)−Pd−Cl(2)	89.5(1)
Pd−Cl(2)	2.306 (3)	Cl(1)−Pd−Cl(2a)	90.5(1)
N−C(1)	1.342 (10)	C(1)−N−C(5)	121.1(8)
N−C(5)	1.343 (13)	C(1)−N−C(6)	118.6(8)
N−C(6)	1.485 (11)	C(5)−N−C(6)	120.2(7)
C(1)−C(2)	1.386 (13)	N−C(1)−C(2)	119.3(9)
C(2)−C(3)	1.372 (17)	N−C(5)−C(4)	120.1(8)
C(3)−C(4)	1.354 (15)	C(1)−C(2)−C(3)	119.9(8)
C(4)−C(5)	1.376 (15)	C(2)−C(3)−C(4)	119.4(9)
		C(3)−C(4)-C(5)	120.1(11)
		$[C16\text{-}Py]_2[PdBr_4]$	
Pd−Br(1)	2.435 (1)	Br(1)−Pd−Br(2)	90.6(1)
Pd−Br(2)	2.419 (1)	Br(1)−Pd−Br(2a)	89.4(1)
N−C(1)	1.324 (10)	C(1)−N−C(5)	120.7(6)
N−C(5)	1.355 (7)	C(1)−N−C(6)	120.1(5)
N−C(6)	1.483 (8)	C(5)−N−C(6)	119.2(6)
C(1)−C(2)	1.380 (12)	N−C(1)−C(2)	120.8(6)
C(2)−C(3)	1.391 (11)	N−C(5)−C(4)	120.5(7)
C(3)−C(4)	1.371 (13)	C(1)−C(2)−C(3)	118.8(9)
C(4)−C(5)	1.346 (10)	C(2)−C(3)−C(4)	118.7(7)
		C(3)−C(4)−C(5)	120.5(7)

sublayers (Figure 2). In the ionic sublayer each $[PdX_4]^{2-}$ anion is sandwiched between two pyridinium rings which are separated from each other by an average

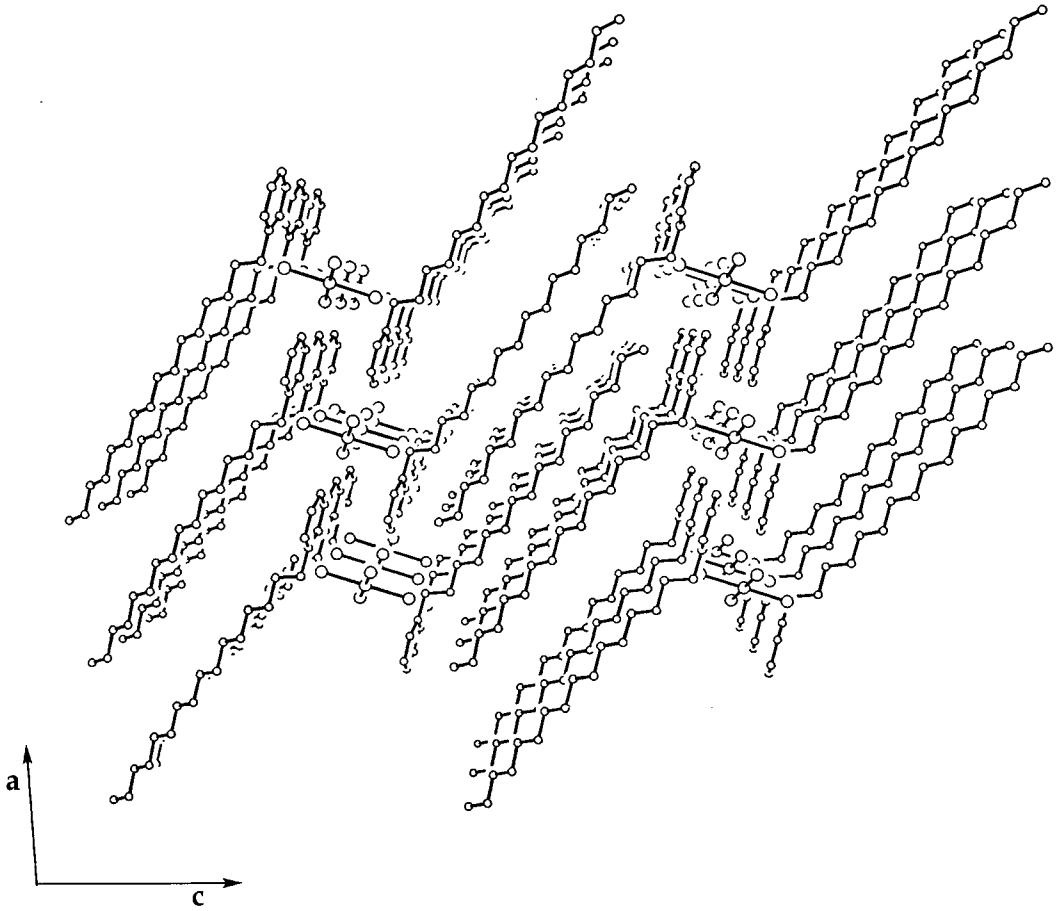

Figure 2. Crystal packing projection of $[C16\text{-}Py]_2[PdCl_4]$ down the *b*-axis.

distance of 5.5 Å in $[C12\text{-}Py]_2[PdCl_4]$, 4.6 Å in $[C16\text{-}Py]_2[PdCl_4]$, and 5.0 Å in $[C16\text{-}Py]_2[PdBr_4]$. The high degree of interdigitation within the paraffinic sublayer is found in all three complex salts as a consequence of the relevant segregation effect of alkyl chains. The long molecular axis is tilted with respect to the layer normal by 47° in $[C12\text{-}Py]_2[PdCl_4]$ and by 50° in both $[C16\text{-}Py]_2[PdCl_4]$ and $[C16\text{-}Py]_2[PdBr_4]$.

All of the halogen atoms of the anion are part of a three-dimensional hydrogen-bonding network, where hydrogen-bonded ring structures are formed within the ionic region.[27] In fact, the presence of H···X contacts shorter than 2.95 or 3.05 Å (the sum of the van der Waals radii of hydrogen and chlorine or bromine atoms,[28] respectively) suggests the existence of possible (C−)H···X hydrogen bonds (Table 5). All of the shortest H···X contacts involve only the hydrogen atoms of the pyridine rings. The local structure around a single cation is shown in Figure 3.

Thermal Properties. The thermal properties of the two homologous series $[Cn\text{-}Py]_2[PdX_4]$ (n = 12, 14, 16, 18; X = Cl, Br) were investigated by hot-stage polarizing optical microscopy and differential scanning calorimetry (DSC). Apart from the two terms with n = 12 which are not mesomorphic, all of the compounds reported in this study show liquid crystalline behavior. However, $[PdCl_4]^{2-}$ and $[PdBr_4]^{2-}$ derivatives behave differently, with the tetrachloropalladate salts showing more pronounced polymorphism. Transition temperatures and phase assignments are reported in Table 6.

Table 5. Short (C)H···X Contacts for $[C12\text{-}Py]_2[PdCl_4]$, $[C16\text{-}Py]_2[PdCl_4]$, and $[C16\text{-}Py]_2[PdBr_4]$

contact[a]	(C−)H···X distance (Å)	C−H···X angle (deg)
	$[C12\text{-}Py]_2[PdCl_4]$	
H(3)···Cl(1^{i})	2.88	154.0
H(4)···Cl(1^{ii})	2.76	138.9
H(1)···Cl(2^{iii})	2.79	158.0
H(5)···Cl(2^{iv})	2.69	160.0
	$[C16\text{-}Py]_2[PdCl_4]$	
H(3)···Cl(1^{v})	2.93	158.1
H(4)···Cl(1^{vi})	2.71	146.1
H(1)···Cl(2^{iii})	2.81	162.9
H(5)···Cl(2^{iv})	2.78	150.4
	$[C16\text{-}Py]_2[PdBr_4]$	
H(5)···Br(1)	3.04	159.7
H(1)···Br(1^{vii})	2.85	155.4
H(2)···Br(2^{vi})	2.81	143.0
H(3)···Br(2^{viii})	3.02	161.2

[a] Symmetry code: (i) $1-x, -y, -z$; (ii) $x+1, y+1, z$; (iii) $-x, -y, -z$; (iv) $-x, 1-y, -z$; (v) $1+x, y, z$; (vi) $-1-x, 1-y, -z$; (vii) $x, y+1, z$; (viii) $x-1, y, z$.

The DSC thermogram of $[C14\text{-}Py]_2[PdCl_4]$ shows three distinct endothermic events around 121, 131, and 132 °C (Figure 4a). Optical observations can confirm only the last two transitions, that is, the formation of a highly viscous, low-birefringent phase followed immediately by clearing to an isotropic liquid. In addition to a similar sequence of thermal events, the higher homologues (n = 16, 18) show a second high-temperature mesophase which invariably appears under crossed

(27) Hitchcock, P. B.; Seddon, K. R.; Welton, T. *J. Chem. Soc., Dalton Trans.* **1993**, 2639.
(28) Taylor, R.; Kennard, O. *J. Am. Chem. Soc.* **1982**, *104*, 5063.

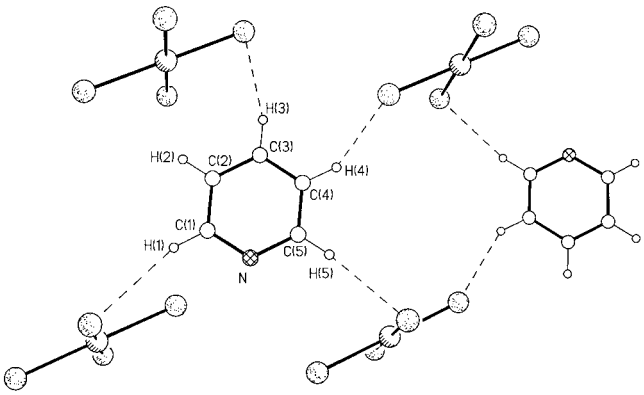

Figure 3. View of [C16-Py]$_2$[PdCl$_4$] showing the (C−)H···Cl contacts less than 2.95 Å.

polarizers with an oily streak texture and large pseudoisotropic areas. Whereas partial degradation always occurs just before the isotropization of the higher homologues (n = 16, 18), all of the remaining transitions are reversible for several heating−cooling cycles provided the decomposition temperature is not approached.

The series of [PdBr$_4$]$^{2-}$ salts has a simpler mesomorphic behavior which in a way mirrors that of the [PdCl$_4$]$^{2-}$ analogues. Thus, with increasing n a nonmesomorphic short analogue (n = 12) is followed by a monotropic one (n = 14) and two enantiotropic analogues (n = 16, 18). The single mesophase of [Cn-Py]$_2$[PdBr$_4$] (n = 16, 18) appears with an oily streak texture along with large pseudoisotropic regions. [C14-Py]$_2$[PdBr$_4$] shows small areas with a focal-conic texture on cooling from the isotropic melt while most of the sample remains homeotropic.

Beside the liquid crystalline phase, the higher homologues (n = 16, 18) show a crystal-to-crystal transition which can be revealed by DSC but is not evident by optical microscopy. In the case of [C16-Py]$_2$[PdBr$_4$], which has the higher stability toward decomposition of the two, the crystal-to-crystal transition is no longer visible in the DSC trace of a second heating cycle (Figure 4b). Meanwhile, the sharp DSC peak at 120 °C corresponding to the melting transition (first heating cycle, ΔH = 75.6 kJ mol^{-1}) becomes broader (ΔH = 54.5 kJ mol^{-1}) and shifts to lower temperature (112 °C). Such a difference might well be related to slight decomposition.

From a quick comparison of the mesomorphism of the two series [Cn-Py]$_2$[PdCl$_4$] and [Cn-Py]$_2$[PdBr$_4$] (n = 14, 16, 18), two major differences immediately arise: (i) [PdCl$_4$]$^{2-}$ derivatives enter a low-temperature ordered smectic phase before eventually melting into a smectic

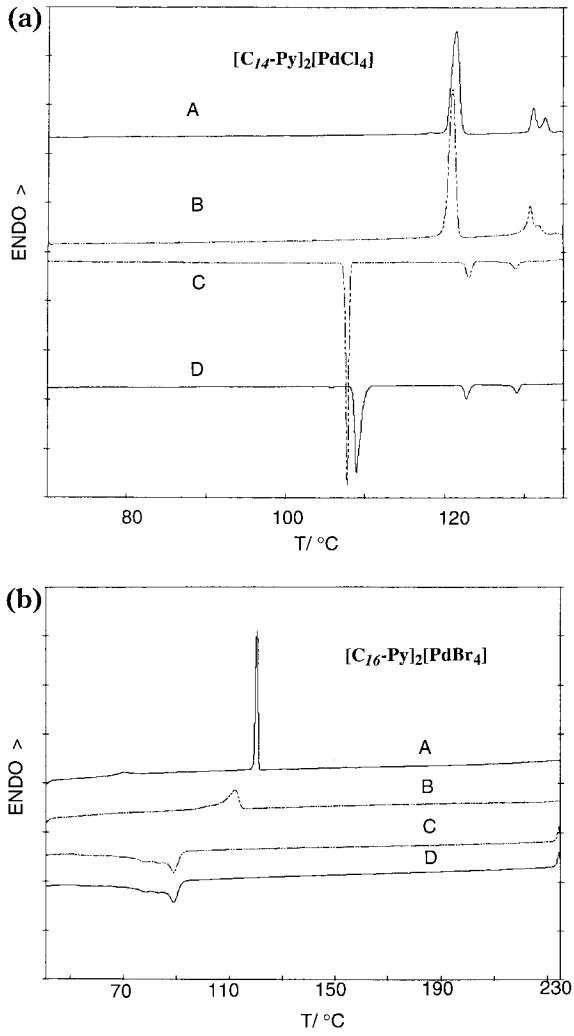

Figure 4. DSC traces of (a) [C14-Py]$_2$[PdCl$_4$] and (b) [C16-Py]$_2$[PdBr$_4$] recorded with a heating rate of 5 °C min^{-1}. (A) First heating; (B) second heating; (C) second cooling; (D) first cooling.

phase with liquid layers; (ii) the highest enthalpy of transition is related to the melting transition for the [PdBr$_4$]$^{2-}$ derivatives, as opposed to a crystal-to-crystal transition for the [PdCl$_4$]$^{2-}$ salts. Moreover, for both series the temperature of the major structural event barely depends on n, while its enthalpy steadily increases with n.

The thermal behavior of the series [Cn-Py]$_2$[PdCl$_4$] (n = 12, 14, 16, 18) should also be compared with that of the corresponding [Cn-Py]$_2$[MCl$_4$] (M = Co, Ni; n = 12, 14, 16, 18) series.[5] From such a comparison it becomes evident that the latter salts show a better thermotropic

Table 6. Transition Temperatures for [Cn-Py]$_2$[PdX$_4$] Complex Species (n = 12, 14, 16, 18; X = Cl, Br) (ΔH, in kJ mol^{-1}, in Parentheses) As Determined by DSC

X	n	K		K′		S_E		S_{Ad}		I
Cl	12	•							121.0 (59.9)	•
	14[b]	•	121.4 (51.5)	•	131.3 (13.1)[c]	•			132.1 (13.1)[c]	•
	16[d]	•	123.4 (66.2)	•	129.3 (7.1)	•	156.8 (8.2)	•	230 (dec)	•
	18[d]	•	123.3 (82.8)	•	126.0 (7.4)	•	167.0 (9.1)	•	232 (dec)	•
Br	12	•							113.0 (52.0)	•
	14	•							114.6 (50.4)	•
	16[b]	•	70.1 (5.9)	•			119.9 (75.6)	•	221[e]	•
	18	•	82.0 (7.5)	•			121.9 (90.2)	•	260.0 (1.0)[f]	•

[a] K = crystal; S = smectic; I = isotropic liquid. [b] Scanning rate of 5 °C min^{-1}. [c] Total ΔH value. [d] Scanning rate of 2 °C min^{-1}. [e] As seen by polarizing optical microscopy. [f] Partial decomposition.

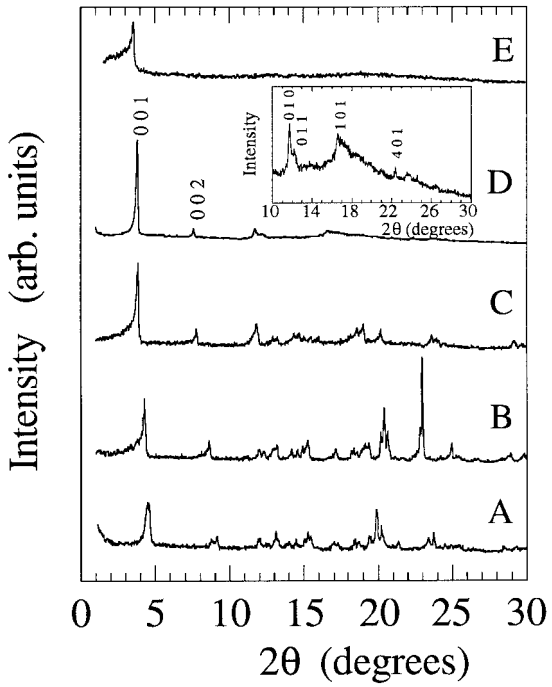

Figure 5. Variable-temperature powder XRD patterns of $[C16\text{-}Py]_2[PdCl_4]$ in the first heating cycle: (A) $T = 25$ °C; (B) $T = 70$ °C; (C) $T = 125$ °C; (D) $T = 140$ °C; (E) $T = 170$ °C. The inset shows an expanded intensity scale of the wide-angle region ($2\theta > 10°$) of spectrum D.

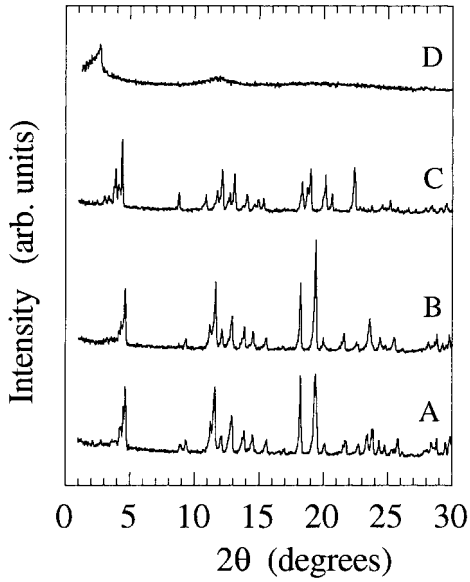

Figure 6. Variable-temperature powder XRD patterns of $[C16\text{-}Py]_2[PdBr_4]$ in the first heating cycle: (A) $T = 25$ °C; (B) $T = 50$ °C; (C) $T = 90$ °C; (D) $T = 125$ °C.

liquid crystal character (mesomorphism spanning a wider *n* range, lower melting temperatures, and no decomposition reported). Although poorly characterized, both the Co(II) and Ni(II) series apparently exhibit a single mesophase throughout the whole temperature range. It is interesting to note that the proposed lamellar (S_A) character of the mesophase[5] is the same as for the high-temperature phase of $[Cn\text{-}Py]_2[PdCl_4]$ ($n = 16, 18$).

Variable-Temperature Powder X-ray Diffraction Measurements. From the results of the optical observations one may conclude that the high-temperature phases of the compounds $[Cn\text{-}Py]_2[PdX_4]$ ($n = 16, 18$; X = Cl, Br) all have the same symmetry. To confirm this assignment and to gain a better understanding of the temperature dependence of the structural changes, we have studied the thermal behavior of the above salts by X-ray diffraction on powdered samples. As representative examples, Figures 5 and 6 show selected X-ray diffraction patterns for $[C16\text{-}Py]_2[PdCl_4]$ and $[C16\text{-}Py]_2[PdBr_4]$, respectively, measured during the first heating cycle.

The room-temperature (RT) crystalline solid phase of $[C16\text{-}Py]_2[PdCl_4]$ (Figure 5, spectrum A) features a lamellar structure corresponding to a periodicity of 18.9 Å, as proved by the presence of a strong diffraction peak in the small-angle region of the spectrum. This phase is stable up to 123 °C, where a crystal-to-crystal phase transition occurs (Figure 5, spectrum C). With increasing temperature, a second transition is observed at 129 °C. The spectrum is now characterized by two sharp Bragg reflections in the small-angle region and a number of sharp wide-angle peaks of low intensity (Figure 5, spectrum D). The small-angle diffraction peaks correspond to a well-organized layered structure, with spacing $d = 23.0$ Å, whereas the wide-angle features might be consistent with the positional order of a crystal smectic mesophase. A further temperature increase leads to the formation of a disordered smectic phase above 157 °C (Figure 5, spectrum E). This final mesophase has a layer spacing $d = 30.8$ Å (at $T = 160$ °C) and is characterized by a degree of longitudinal correlation lower than that in the previous smectic phase, as indicated by the appreciable broadening of the small-angle diffraction peak. Only a slight increase of the layer spacing is observed with further increases of the temperature up to the clearing point. A very similar X-ray sequence was observed for the sample $[C18\text{-}Py]_2[PdCl_4]$. In this case, the layer spacings in the ordered and disordered smectic mesophases are 25.6 and 34.3 Å, respectively. These values are greater than those found for the corresponding mesophases in $[C16\text{-}Py]_2[PdCl_4]$, which is consistent with the lengthening of the hydrocarbon chains.

A different mesophase sequence was observed for the sample $[C16\text{-}Py]_2[PdBr_4]$. The lamellar structure of the RT crystalline solid phase of this sample is apparent from the small-angle sharp reflection in Figure 6, spectrum A. The RT diffraction pattern remains unaffected (Figure 6, spectrum B) until a crystal-to-crystal phase transition occurs at 70 °C (Figure 6, spectrum C). A further temperature increase above 120 °C shows the formation of a disordered smectic mesophase with layer thickness $d = 31.6$ Å (Figure 6, spectrum D). The broad, weak, and diffuse signal centered at $2\theta \approx 12°$ in Figure 6, spectrum D, is associated with the short-range positional correlation of the $[PdBr_4]^{2-}$ anions within the smectic planes; the corresponding correlation length is ~7.5 Å. Very similar mesophase behavior was observed for the sample $[C18\text{-}Py]_2[PdBr_4]$. For this salt, the layer spacing in the smectic mesophase is $d = 35.3$ Å, whereas the lengthening of the hydrocarbon chains has no effect on the in-plane correlation length.

Table 7. Lattice Parameters of Crystalline (K and K′) and Smectic E Phases for Given Temperatures, *T*

			cell parameters					
	T (deg)	crystal system	*a* (Å)	*b* (Å)	*c* (Å)	α (deg)	*β* (deg)	*γ* (deg)
[C16-Py]$_2$[PdCl$_4$]	25 (K)	triclinic	7.85	8.07	19.09	96.1	93.1	104.0
	126 (K′)	triclinic	6.31	6.99	22.64	96.7	90.6	103.6
	140 (S_E)	orthorhombic	5.48	7.49	22.98			
[C18-Py]$_2$[PdCl$_4$]	25 (K)	triclinic	7.21	7.84	20.39	97.8	94.1	99.8
	124 (K′)	triclinic	6.26	7.54	25.20	90.6	92.7	90.4
	126 (S_E)	orthorhombic	5.48	7.86	25.78			
[C16-Py]$_2$[PdBr$_4$]	25 (K)	triclinic	7.97	8.21	19.05	96.1	93.7	105.0
	90 (K′)	triclinic	7.53	8.41	20.07	89.6	92.5	104.8
[C18-Py]$_2$[PdBr$_4$]	25 (K)	triclinic	7.60	8.18	20.67	82.3	86.1	71.4
	100 (K′)	triclinic	7.59	8.45	21.65	89.2	88.4	75.2

Discussion

The study of the temperature dependence of the structural changes of the two homologous series [C*n*-Py]$_2$[PdX$_4$] (X = Cl, Br) has shown that (i) the two series behave independently, with the [PdCl$_4$]$^{2-}$ series showing the richest polymorphism; (ii) the mesomophase temperature ranges of twin terms (equal *n* values) have similar values, although the [PdCl$_4$]$^{2-}$ salts usually have the highest melting and clearing temperatures; and (iii) when mesomorphic, [PdBr$_4$]$^{2-}$ salts are less prone to decomposition around the clearing transition. All of these observations seem to point to a propensity to give mesophases in the order [PdBr$_4$]$^{2-}$ > [PdCl$_4$]$^{2-}$. Other observations, however, are at odds with the above order. For example, though observed over a very short range, the enantiotropic mesomorphism of [C14-Py]$_2$[PdCl$_4$] vs the monotropic behavior of [C14-Py]$_2$[PdBr$_4$ is contrary to the above trend. A confirmation of the trend reversal may be found in the additional observation that the ad hoc synthesized salt [C14-Py]$_2$[PdI$_4$] shows no mesomorphism at all (K → I at 101.0 °C).

That the mesomorphism of complex metal salts depends on the type of anions (and the length of the alkyl chains) is not a new and original idea, yet the reasons for the specific behavior in a specific case are not always understood. As for many nonionic amphiphiles,[29] hydrogen bonding may in this case (and for related species)[6] make an important contribution to the stabilization of an individual mesophase. What is not clear is the extent to which such a contribution is important. An in-depth analysis of the VT-XRD data for the studied samples sheds further light on the thermal behavior of the whole series.

The powder X-ray spectra of [C*n*-Py]$_2$[PdX$_4$] (*n* = 16, 18; X = Cl, Br) can be easily indexed except for the high-temperature disordered mesophase. The crystal system and the unit cell parameters are summarized in Table 7. The corresponding X-ray interlayer spacings are shown in Table 8. In all cases the crystalline solid phase at room temperature (K) is triclinic and is characterized by a quasi-single-layered structure with a layer thickness always less than the corresponding *L* value. Symmetry considerations led us to prefer the estimated lengths *L* (Figure 7) both to the calculated length of a single pyridinium cation and to the calculated length of a salt unit (*l* in Figure 7) each with alkyl chains in their most extended conformation.[30] Ordering of the isolated alkyl chains in the smectic-like *ab*-plane is hexagonal close-packed. Following the first DSC thermal event (first heating cycle), the diffraction data reveal a change to a second triclinic solid phase (K′) for both [PdCl$_4$]$^{2-}$ and [PdBr$_4$]$^{2-}$ salts. However, a large increase (between 19% and 25%) of the interlayer spacing *d* is observed only for the [PdCl$_4$]$^{2-}$ salts, which leads to a partial loss of interdigitation between alkyl chains (Figure 8). This is in good agreement with the observation of a large ΔH value for the transition, although the crystal system remains the same. For [C18-Py]$_2$[PdCl$_4$] there was also an alternative possibility that the solid phase might belong to the monoclinic system (α and $\gamma \approx 90°$). Indexing of the XRD pattern to this system, however, failed to give reasonable unit cell parameters.

A further increase in temperature causes the transition to an ordered smectic phase for [C16-Py]$_2$[PdCl$_4$] and [C18-Py]$_2$[PdCl$_4$], which is related to a rather small (between 1.6% and 2.7%) change of the *d* value.Two sharp diffraction peaks at low angles are easily indexed to the (001) and (002) reflections of a layered smectic

Table 8. Interlamellar Spacings of Crystalline and Smectic Phases for Given Temperatures, *T*, with Calculated *L* Values for Comparison

	L (Å)	*T* (°C)	*d*(K) (Å)	*d*(K′) (Å)	*d*(S_E) (Å)	*d*(S_{Ad}) (Å)
[C16-Py]$_2$[PdCl$_4$]	19.7	25	18.9	22.5	23.1	30.8
		125				
		140				
		160				
[C18-Py]$_2$[PdCl$_4$]	22.3	25	20.1	25.2	25.6	34.3
		124				
		126				
		180				
[C16-Py]$_2$[PdBr$_4$]	19.7	25	18.9	20.1		31.6
		90				
		125				
[C18-Py]$_2$[PdBr$_4$]	22.3	25	20.5	21.7		35.4
		100				
		130				

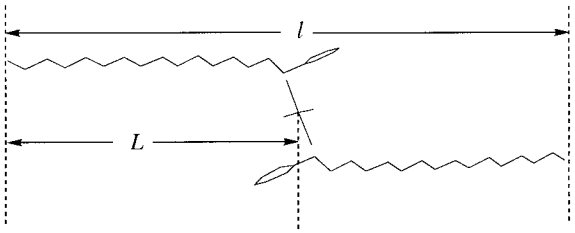

Figure 7. Schematic representation of a [C*n*-Py]$_2$[PdX$_4$] salt unit. The *l* and *L* lengths (where $L = l/2$) are estimated from solid-state crystallographic data for $n = 12$ and 16.

(29) Paleos, C. M.; Tsiourvas, D. *Angew. Chem., Int. Ed. Engl.* **1995**, *34*, 1696.

(30) This choice rules out the need for considering separate contributions of both the cations and the anion to the calculated length of the molecules.

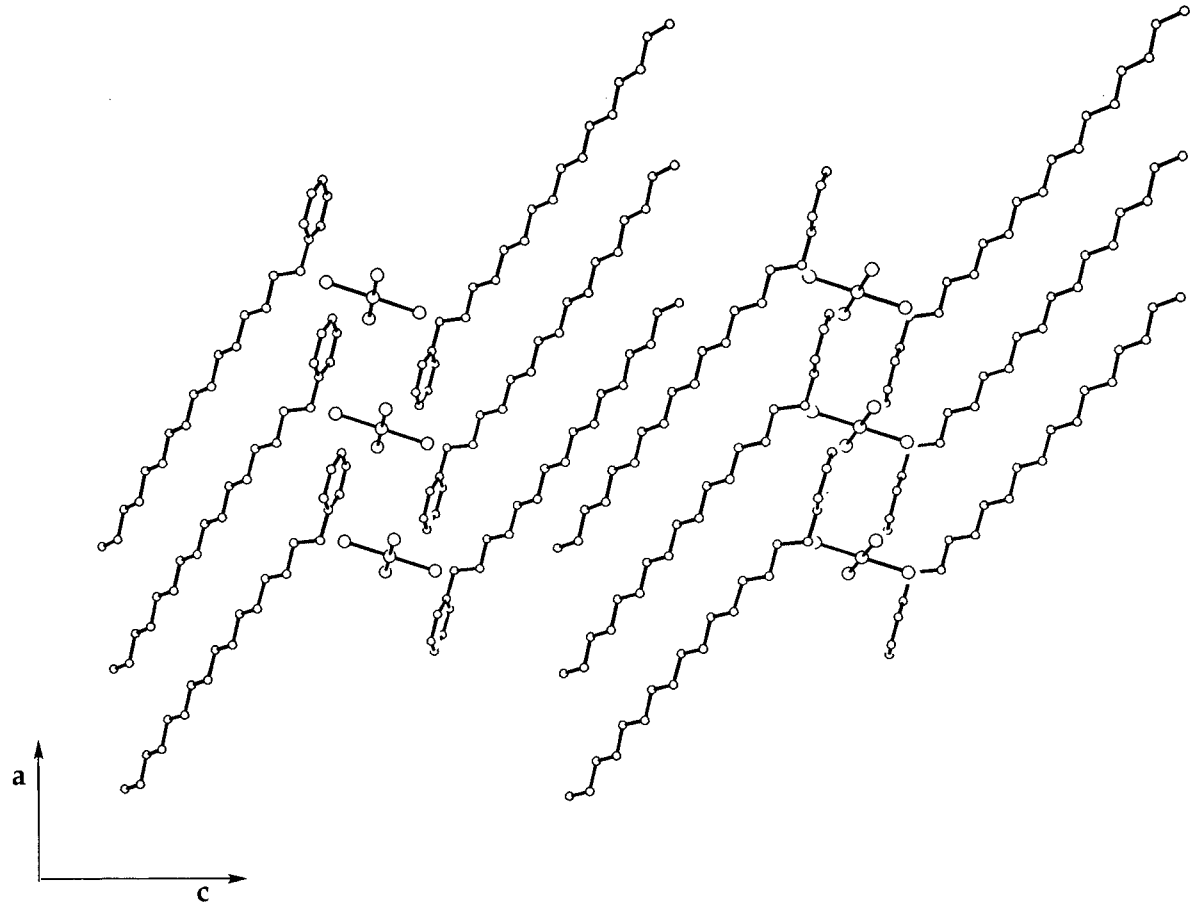

Figure 8. Crystal packing of $[C16\text{-}Py]_2[PdCl_4]$ down the *b*-axis in the triclinic solid-phase K′ at 125 °C.

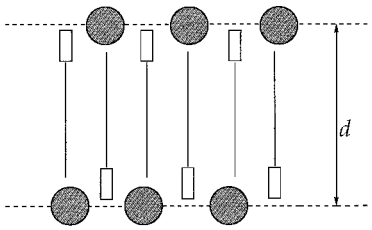

Figure 9. Schematic representation of a single layer of the smectic E mesophase for $[Cn\text{-}Py]_2[PdCl_4]$ species. Horizontal dashed lines define the thickness of the layer, circles refer to the anions, and rectangles represent the pyridinium cores.

structure (see Figure 5, spectrum D, for $[C16\text{-}Py]_2[PdCl_4]$), whereas the positional ordering within the layers results from indexing of the scattering signals in the wide-angle region of the X-ray patterns. In both salts an orthorhombic lattice is obtained with unit cell parameters as reported in Table 7. This symmetry is consistent only with an orthogonal crystal smectic E phase.[31] A similar phase is also likely for the high-temperature phase of $[C14\text{-}Py]_2[PdCl_4]$, which has not been studied by VT-XRD due to the very narrow mesophase temperature range. A schematic representation of the arrangement of ions in the smectic layer of the S_E phase is proposed in Figure 9. The fact that the interlayer distance determined from XRD (Table 7) is somewhat larger than *L* is not a problem viewed in terms of a mesophase model in which the cations are in a head-to-head arrangement with stiff and highly interdigitated alkyl chains (Figure 9), a model which is reminiscent of the lyotropic lamellar β phase (L_β).[32]

On further warming of the $[Cn\text{-}Py]_2[PdX_4]$ ($n = 16$, 18; X = Cl, Br) salts, both the intralayer and the interlayer registries are lost in favor of a smectic A mesophase with similar interlayer spacings for the analogous terms of the two pairs of salts (Table 8). This final mesophase is best assigned to a partially bilayered (A_d) phase,[31] as the observed *d* values are in the range $L < d < 2L$. In conclusion, two different structural transformations have been observed for the $[PdCl_4]^{2-}$ and $[PdBr_4]^{2-}$ salts. Whereas the first (crystal → crystal′ → ordered smectic → disordered smectic) shows the highest ΔH at the crystal → crystal′ transition, in the second (crystal → crystal′ → disordered smectic) the highest ΔH corresponds to the melting event.

Since the additional contribution of the hydrogen bonds to the response of the ionic system to the increase in thermal energy on heating may parallel the order of the strength of the (C−)H···X hydrogen bonds, weaker bonds (as for the $[PdBr_4]^{2-}$ salts) should make the appearance of mesomorphism easier. On the other hand, both the ionic forces and the hydrophobic effect are largely responsible for the thermotropic mesomorphism. Hence, whereas hydrogen bonding is a crucial factor in the mesomorphism of nonionic amphiphiles such as carbohydrate[33] or polyhydroxy[34] mesogens in

(31) Chandrasekkar, S. *Liquid Crystals*, 2nd ed.; Cambridge University Press: Cambridge, 1992.

(32) Tardieu, A.; Luzzati, V.; Reman, F. C. *J. Mol. Biol*. **1973**, *75*, 711.

(33) Jeffrey, J. A.; Wingert, L. M. *Liq. Cryst*. **1992**, *12*, 179.

(34) Hentrich, F.; Diele, S.; Tschierske, C. *Liq. Cryst*. **1994**, *17*, 827.

general, in the $[Cn\text{-}Py]_2[PdX_4]$ species it is more a destabilizing contribution than a stabilizing factor. In short, hydrogen bonding mostly stabilizes the crystalline state or delays the disordering of the ionic sublayer in the ordered mesophase. No relevant part in the stabilization of the disordered mesophase is expected.

With reference to the tetrahalometalate anion, size effects also become increasingly important in the order $[PdCl_4]^{2-} < [PdBr_4]^{2-} < [PdI_4]^{2-}$. At this stage, however, it is impossible to evaluate correctly the importance of geometry effects on the mesomorphic properties. This is because careful studies on the thermotropic mesomomorphism of $[Cn\text{-}Py]_2[MX_4]$ species with tetrahedral or distorted square-planar $[MX_4]^{2-}$ anions[5] are not available yet.

Acknowledgment. Financial support from the Italian Ministero dell'Università e della Ricerca Scientifica e Tecnologica (MURST) and Consiglio Nazionale delle Ricerche (CNR) is gratefully acknowledged.

Supporting Information Available: Full distance and angle listings (SI−SIII), hydrogen coordinates (SIV−SVI) and anisotropic temperature factors (SVII−SIX) for compounds $[C12\text{-}Py]_2[PdCl_4]$, $[C16\text{-}Py]_2[PdCl_4]$, and $[C16\text{-}Py]_2[PdBr_4]$ (9 pages); structure factor tables (42 pages). Ordering information is given on any current masthead page.

CM980071L